

Probing coherent Cooper pair splitting with cavity photons

Audrey Cottet

*Laboratoire Pierre Aigrain, Ecole Normale Supérieure, CNRS UMR 8551,
Laboratoire associé aux universités Pierre et Marie Curie et Denis Diderot,
24, rue Lhomond, 75231 Paris Cedex 05, France*

This work discusses theoretically the behavior of a microwave cavity and a Cooper pair beam splitter (CPS) coupled non-resonantly. The cavity frequency pull is modified when the CPS is resonant with a microwave excitation. This provides a direct way to probe the coherence of the Cooper pair splitting process. More precisely, the cavity frequency pull displays an anticrossing whose specificities can be attributed unambiguously to coherent Cooper pair injection. This work illustrates that microwave cavities represent a powerful and qualitatively new tool to investigate current transport in complex nanocircuits.

PACS numbers: 73.23.Hk, 74.45.+c, 73.63.Fg, 03.67.Bg

I. INTRODUCTION

Superconductors represent a natural source of entanglement due to Cooper pairs which gather two electrons in the spin singlet state. The spatial separation of these electrons is an interesting goal in the context of quantum computation and communication. In principle, a Cooper pair beam splitter (CPS) connected to a central superconducting contact and two outer normal metal (N) contacts could facilitate this process¹. The spatial splitting of Cooper pairs has been demonstrated experimentally from an analysis of the CPS average currents, current noise and current cross-correlations^{2,3}. However, new tools appear to be necessary to investigate further the CPS dynamics, and in particular its coherence, which has not been demonstrated experimentally so far^{4,5}. This coherence has two intimately related aspects: the coherence of Cooper pair injection and the conservation of spin-entanglement. The first aspect is due to the fact that Cooper pair injection into the CPS is a coherent crossed Andreev process, which produces a coherent coupling between the initial and final states of the Cooper pair in the superconducting contact and the CPS (see e.g.^{6,7}). The observation of coherent pair injection appears as an important prerequisite for the realization of a fully coherent CPS.

In Cavity Quantum Electrodynamics (QED)^{8,9} or Circuit QED¹⁰, real or artificial two levels atoms are controlled and readout at an exquisite level thanks to the use of cavity photons. Very recently, coplanar microwave cavities have been coupled to nanocircuits based on carbon nanotubes (CNTs), semiconducting nanowires or two-dimensional electron gases^{11–14}. This paves the way for the development of a Hybrid Circuit QED which offers many possibilities due to the versatility of nanocircuits made with nanolithography techniques. Indeed, nanoconductors can be coupled to various types of reservoirs such as normal metals, ferromagnets¹⁵ or superconductors¹⁶, in a large variety of geometries^{17–22}. Hybrid Circuit QED tackles problems which go beyond the mechanics of closed two level

systems. In particular, the interaction between electronic transport and the light-matter interaction leads to a rich phenomenology^{18,21–23}. Photon emission in the cavity/nanoconductor resonant regime has retained most attention so far. In contrast, this work considers a CPS and a cavity coupled non-resonantly, so that the CPS simply causes a cavity frequency pull. When the CPS is excited with a microwave voltage, the cavity frequency pull displays an anticrossing which can be attributed unambiguously to coherent Cooper pair injection, due to various specificities related to the transport geometry and the symmetries of the split singlet Cooper pairs. More generally, our work illustrates that Hybrid Circuit QED provides a powerful and qualitatively new tool to investigate current transport in complex nanocircuits.

II. HAMILTONIAN DESCRIPTION OF THE CPS AND CAVITY

I consider a CNT (light blue) placed between the center and ground conductors (purple) of a superconducting coplanar waveguide cavity (Fig. 1.a). A grounded superconducting contact (purple) and two outer N contacts (black) biased with a voltage V_b are used to define two quantum dots L and R along the CNT. The dot $L(R)$ is placed close to a gate electrode (gray) biased with a DC voltage $V_g^{L(R)}$. I use the CPS hamiltonian

$$H_{CPS} = \sum_{i,\tau,\sigma} \left((\varepsilon + \Delta_{so}\tau\sigma) d_{i\tau\sigma}^\dagger d_{i\tau\sigma} + \frac{\varepsilon_B}{2} d_{i\tau\sigma}^\dagger d_{i\tau\bar{\sigma}} \right) + \Delta_{K \leftrightarrow K'} \sum_{i,\sigma} (d_{iK\sigma}^\dagger d_{iK'\sigma} + h.c.) + t_{ee} \sum_{\tau,\sigma} (d_{L\tau\sigma}^\dagger d_{R\tau\sigma} + h.c.) + H_{prox} + H_{int} \quad (1)$$

with

$$H_{prox} = t_{eh} \sum_{\tau} \left(d_{L\tau\uparrow}^\dagger d_{R\bar{\tau}\downarrow}^\dagger - d_{L\bar{\tau}\downarrow}^\dagger d_{R\tau\uparrow}^\dagger \right) + h.c. \quad (2)$$

The operator $d_{i\tau\sigma}^\dagger$ creates an electron with spin $\sigma \in \{\uparrow, \downarrow\}$ along the CNT axis, in orbital $\tau \in \{K, K'\}$ of dot $i \in \{L, R\}$. The twofold orbital degeneracy is due to the

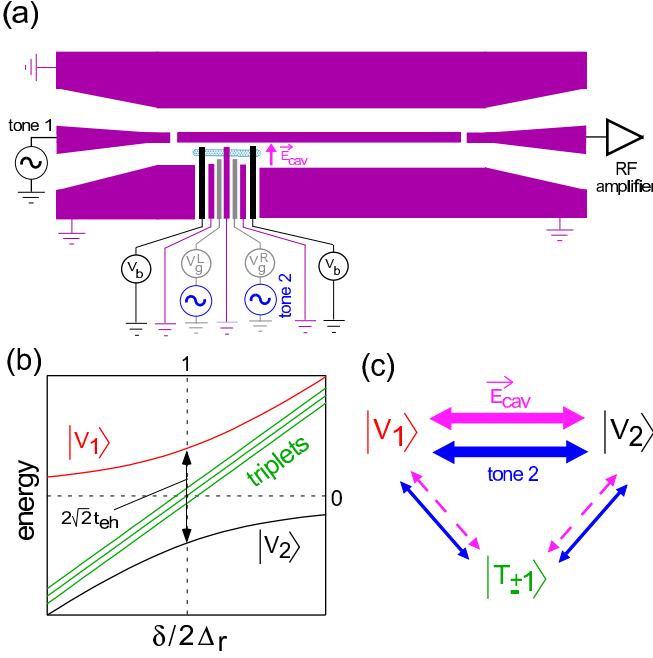


FIG. 1: (a) Scheme of the CPS embedded in a coplanar microwave cavity (for details, see text). (b) Energy levels of the subspace \mathcal{E} near $\delta \sim 2\Delta_r$. (c) Scheme of the couplings between some states of \mathcal{E} , provided by the cavity electric field (pink arrows) and the classical tone 2 (blue arrows). The couplings corresponding to the dashed arrows can be disregarded in our study (see text).

atomic structure of the CNT. The term in Δ_{so} is caused by spin-orbit coupling²⁴. The term in $\Delta_{K \leftrightarrow K'}$ describes a coupling between the K and K' orbitals, due to disorder in the CNT atomic structure^{24–27}. The term in t_{ee} describes interdot hopping. An external magnetic field \vec{B} is applied in the plane of the cavity, perpendicular to the CNT. This produces a Zeeman splitting $\varepsilon_B = g\mu_B B$ of the spin states in the dots. The term H_{int} describes Coulomb interactions inside the CPS. The term in t_{eh} describes the coherent injection of singlet Cooper pairs inside the CPS. This approach disregards single quasiparticle transport between the superconducting contact and the dots, which is reasonable for subgap bias voltages⁷. The total hamiltonian describing the CPS and the cavity is

$$H_{tot} = H_{CPS} + \hbar\omega_{cav}a^\dagger a + H_c + H_{bath} \quad (3)$$

where a^\dagger creates a cavity photon. The term H_c describes the CPS/cavity coupling and H_{bath} describes the coupling of the CPS and cavity to dissipative baths, including the N reservoirs and their DC voltage bias. The amplitude of the cavity electric field can be expressed as $E_{cav} = V_{rms}(a + a^\dagger)/\ell$ with V_{rms} a characteristic voltage and ℓ the distance between the ground and center conductors of the cavity. Due to the imperfect screening of E_{cav} by the CNT, the coupling between the CPS and the

cavity can occur through three paths, i.e. $H_c = h_c(a + a^\dagger)$ with

$$h_c = \sum_{i,\tau,\sigma} \left(\beta_i n_{i\tau\sigma} d_{i\tau\sigma}^\dagger d_{i\tau\sigma} + i\sigma \lambda_i d_{i\tau\sigma}^\dagger d_{i\tau\bar{\sigma}} + \alpha_i d_{i\tau\sigma}^\dagger d_{i\bar{\tau}\sigma} \right) \quad (4)$$

The first term of H_c describes a shift of the chemical potential of dot i proportionally to the cavity electric field \vec{E}_{cav} . The second[third] term describes a coupling of the electrons motion to \vec{E}_{cav} , which enables photon-induced spin-flips [orbit-changes] due to spin-orbit interaction [atomic disorder] in the CNT^{18,27}. The coefficients β_i , λ_i and α_i can be calculated microscopically in a consistent way, by assuming for instance that \vec{E}_{cav} is uniform on the scale of the CPS²⁸.

Due to H_{int} , it is possible to tune $V_g^{L(R)}$ such that there is a single electron on each dot when $V_b = 0$ and $t_{eh} = 0$. I note δ the charging energy corresponding to such an occupation, with respect to the charging energy for having the CPS empty state $|0,0\rangle$. One can tune δ with $V_g^{L(R)}$. When t_{eh} , $\varepsilon_B \ll \Delta_r$ and $\delta \sim 2\Delta_r$ with $\Delta_r = \sqrt{\Delta_{so}^2 + \Delta_{K \leftrightarrow K'}^2}$, one can isolate an ensemble $\mathcal{E} = \{|V_1\rangle, |V_2\rangle, |T_+\rangle, |T_-\rangle, |T_0\rangle\}$ of five CPS even-charged eigenstates which are below all other even-charged eigenstates, by an energy $\sim 2\Delta_r$ at least. The eigenstates $|V_1\rangle$ and $|V_2\rangle$ are a coherent superposition of $|0,0\rangle$ and a spin singlet state $|S\rangle$, due to the term in t_{eh} . The states $|S\rangle$ and $|T_n\rangle$, with $n \in \{-1, 0, 1\}$, are generalized spin singlet and spin triplet states, whose definition takes into account the existence of the K/K' orbital degeneracy (see Appendix A). The energy of the different states of \mathcal{E} is given by

$$E_{V_{1(2)}} = \frac{1}{2} \left(\delta - 2\Delta_r \pm \sqrt{8t_{eh}^2 + (\delta - 2\Delta_r)^2} \right) \quad (5)$$

and

$$E_{T_n} = \delta - 2\Delta_r + n \frac{\Delta_{K \leftrightarrow K'}}{\Delta_r} \varepsilon_B \quad (6)$$

As visible in Eq.(5), the states $|V_1\rangle$ and $|V_2\rangle$ form an anticrossing with a width $2\sqrt{2}t_{eh}$ at $\delta \sim 2\Delta_r$ (see Fig.1.b). This anticrossing directly reveals the coherence of the Cooper pair injection process. It is thus crucial to be able to identify this feature in an experiment. In this work, we show that the microwave cavity represents a powerful tool to perform this task.

The states of \mathcal{E} are coupled by cavity photons. I note σ_{cd} the transition operator from states d to c and $\omega_{cd} = (E_c - E_d)/\hbar$. Inside \mathcal{E} , the cavity/CPS coupling writes

$$H_c = eV_{rms} \sum_{cd} \alpha_{cd} \sigma_{cd} (a + a^\dagger) \quad (7)$$

with

$$\alpha_{T_{\pm}V_{1(2)}} = \mp v_{1(2)} i(\lambda_L - \lambda_R) \Delta_{K \leftrightarrow K'} / \Delta_r \sqrt{2} \quad (8)$$

$$\alpha_{T_{\pm}T_0} = i(\lambda_L + \lambda_R) \Delta_{K \leftrightarrow K'} / \Delta_r \sqrt{2} \quad (9)$$

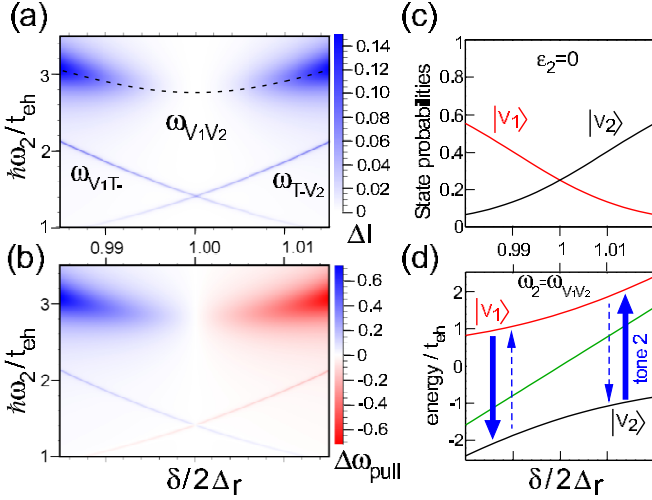


FIG. 2: (a) Current variation ΔI versus δ and ω_2 for $\varepsilon_B = 0$ and a negligible relaxation between the states of \mathcal{E} (b) Corresponding $\Delta\omega_{pull}$ (c) Occupation probabilities of states $|V_1\rangle$ and $|V_2\rangle$ for $\varepsilon_2 = 0$ (d) Scheme illustrating that tone 2 lifts the current blockade through the CPS at both sides of $\delta = 2\Delta_r$. We have used the realistic parameters $t_{eh} = 12 \mu\text{eV}$, $\Delta_{so} = 0.15 \text{ meV}$, $\Delta_{K/K'} = 0.45 \text{ meV}$, $\Gamma_N = 125 \text{ MHz}$, $\omega_{cav} = 2\pi \times 10 \text{ GHz}$, $V_{rms} = 4 \mu\text{eV}$, $\varepsilon_2 = 150 \mu\text{eV}$, $\beta_{L(R)} = 10^{-2}$, $\lambda_L - \lambda_R = 10^{-4}$, and $\alpha_{L(R)} \ll \beta_{L(R)}$. In all the Figs. of this paper, ΔI is reduced by $e\Gamma_N$ and $\Delta\omega_{pull}$ is reduced by the scale ω_0 defined in Eq. (13).

$$\alpha_{V_2 V_1} = v_1 v_2 [(\beta_L + \beta_R) - ((\alpha_L + \alpha_R)\Delta_{K \leftrightarrow K'} / \Delta_r)] \quad (10)$$

$\alpha_{T_0 V_{1(2)}} = 0$ and $\alpha_{cd} = \alpha_{cd}^*$. The term (8) displays destructive interferences between the spin-flip coupling elements λ_L and λ_R because it describes transitions between singlet and triplet states¹⁸. In contrast, (9) depends on $\lambda_L + \lambda_R$ because it describes transitions between triplet states. The term (10) depends on $\beta_L + \beta_R$ because it involves transitions between $|0, 0\rangle$ and $|\mathcal{S}\rangle$, which are triggered by a common oscillation of the two dot levels with respect to the potential of the superconducting contact. It also displays a constructive interference between α_L and α_R .

III. CAVITY FREQUENCY PULL AND CPS INPUT CURRENT IN THE CPS/CAVITY NON-RESONANT REGIME

A. Description of the measurement scheme

Since the couplings $\lambda_{L(R)}$ are expected to be weak, the effects of (8) and (9) should be measurable only when the cavity is closely resonant with the CPS. For instance, Ref.¹⁸ discusses a lasing effect which occurs when $\omega_{V_1 T_{\mp}} = \omega_{cav}$. Such an effect could be challenging to observe because it requires to reach a lasing threshold. For that purpose, it could be necessary to use a cavity with a

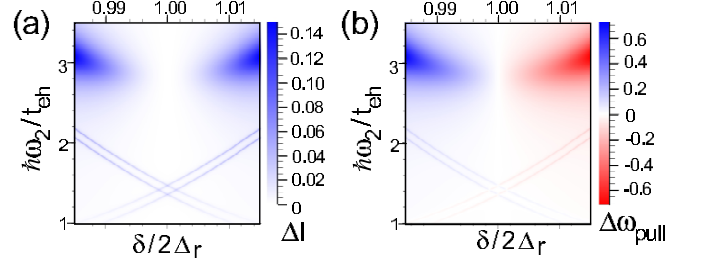


FIG. 3: (a) Current variation ΔI versus δ and ω_2 for B finite. (b) Corresponding $\Delta\omega_{pull}$. We have used the parameters of Fig.2 and $\varepsilon_B = 0.7 \mu\text{eV}$.

high quality factor $Q \geq 10^6$, not achieved yet in Hybrid Circuit QED. This letter discusses the opposite regime, i.e. the cavity and the CPS are non-resonant, so that the CPS can only produce a cavity frequency pull ω_{pull} . This effect is due to an exchange of virtual photons between the CPS and the cavity. Since $\beta_{L(R)} \gg \lambda_{L[R]}$, $\alpha_{L[R]}$ is expected, one can neglect the contribution of (8) and (9) to ω_{pull} . At second order in $\alpha_{V_2 V_1}$, one finds

$$\omega_{pull} = \mathcal{C}\omega_0(P_{V_1} - P_{V_2}) \quad (11)$$

where the probability $P_{V_{1(2)}}$ of state $|V_{1(2)}\rangle$ can be calculated in the absence of the cavity, and the parameters \mathcal{C} and ω_0 are defined as

$$\mathcal{C} = -\frac{2\omega_{cav}\omega_{V_1 V_2}}{\omega_{cav}^2 - \omega_{V_2 V_1}^2} \quad (12)$$

and

$$\omega_0 = (\alpha_{V_2 V_1} eV_{rms})^2 / \omega_{cav} \quad (13)$$

In practice, ω_{pull} can be obtained by measuring the cavity response to a weak microwave drive (tone 1) $H_{d,1} = \varepsilon_1 e^{i\omega_1 t} a + h.c.$ with frequency $\omega_1 \sim \omega_{cav}$ ¹⁰. This will not modify $P_{V_{1(2)}}$ since the cavity and the CPS states are off resonant. Meanwhile, a second microwave drive (tone 2) $H_{d,2} = \sum_{cd} \varepsilon_{2,cd} e^{i\omega_2 t} \sigma_{cd} + h.c.$ with frequency ω_2 can be applied on the CPS gates to control directly the CPS state. For simplicity, one can assume that the electric field \vec{E}_2 associated to tone 2 is parallel to \vec{E}_{cav} and uniform on the scale of the CPS, so that one can use $\varepsilon_{2,cd} = \varepsilon_2 \alpha_{cd}$, with $\varepsilon_2 = e\ell E_2$. One cannot disregard the elements $\varepsilon_{2,cd}$ involving $|T_+\rangle$ or $|T_-\rangle$ because ω_2 can be resonant with any of the CPS transitions.

The present work describes how tone 2 modifies ω_{pull} and the average current I_{CPS} flowing through the CPS superconducting contact for V_b finite. I consider a range of V_b and δ such that electrons can go from the dots to the N reservoirs but not the reverse, and transport processes involve only the states from \mathcal{E} and the CPS singly occupied states¹⁸. Assuming that the bare coupling rate Γ_N between the dots and the N reservoirs is

independent from i , τ , and σ , the details on the CPS singly occupied states are unnecessary to describe electronic transport. In the context of circuit QED and quantum information processing, the limit $\Gamma_N \ll k_B T \ll t_{eh}$ is particularly relevant since it is desirable that electrons stay a long time in the CPS to enable their quantum manipulation. In this case, one can calculate the probability P_c of a state $|c\rangle \in \mathcal{E}$ and the global probability P_s of the CPS singly occupied states from the stationary master equation $(M + M_{rel} + M_{RF})P = 0$ with $P = {}^t\{P_{V_1}, P_{V_2}, P_{T_+}, P_{T_-}, P_{T_0}, P_s\}$. The matrix M takes into account tunnel processes towards the N contacts. Its finite elements are $M_{sV_i} = 2v_i^2\Gamma_N$, $M_{V_i s} = (1 - v_i^2)\Gamma_N$, $M_{sT_i} = 2\Gamma_N$, $M_{V_i V_i} = -2v_i^2\Gamma_N$, $M_{T_i T_i} = -2\Gamma_N$ and $M_{ss} = -\Gamma_N$, with $v_i \in [0, 1]$ a dimensionless coefficient which depends on δ (see Appendix A). The matrix M_{rel} takes into account relaxation processes between the states of \mathcal{E} , due e.g. to phonons. One can use a rotating wave approximation (RWA) on independent resonances²⁹ to describe the effect of tone 2 through the matrix M_{RF} , with, for $(c, d) \in \mathcal{E}^2$,

$$M_{RF,cd} = |\varepsilon_{2,cd}|^2 (2\Gamma_{cd}/(\omega - |\omega_{cd}|)^2 + \Gamma_{cd}^2)/\hbar^2 \quad (14)$$

Above, Γ_{cd} corresponds to the decoherence rate between the states $|c\rangle$ and $|d\rangle$. Assuming that Γ_{cd} is limited by relaxation inside \mathcal{E} and tunnel processes, one can use $\Gamma_{cd} = -(M_{cc} + M_{rel,cc} + M_{dd} + M_{rel,dd})/2$. In the following, I assume that ω_2 is much larger than $\varepsilon_B \Delta_{K \leftrightarrow K'}/\Delta_r$, and I thus disregard the elements $M_{RF,T_0 T_{+[-]}}$. This implies that $|T_0\rangle$ is not populated in the regimes considered below.

Figures 2 to 4 show the variation $\Delta I_{CPS} = I_{CPS}(\varepsilon_2) - I_{CPS}(\varepsilon_2 = 0)$ of the CPS input current $I_{CPS} = e\Gamma_N[2v_1^2, 2v_2^2, 2, 2, 2, 1].P$ and the variation $\Delta\omega_{pull} = \omega_{pull}(\varepsilon_2) - \omega_{pull}(\varepsilon_2 = 0)$ of the cavity frequency pull, versus δ and ω . Various resonant lines are visible in ΔI_{CPS} and $\Delta\omega_{pull}$, for ω_2 equal to $\omega_{V_1 V_2}$, $\omega_{V_1 T_{\pm}}$, and $\omega_{V_2 T_{\pm}}$. Although $\Delta\omega_{cav}$ is dominated by the charge coupling $\alpha_{V_2 V_1}$ to the cavity, it indirectly reveals spin-flip transitions $|V_{1(2)}\rangle \rightleftharpoons |T_{\pm}\rangle$ induced by tone 2, due to a modification of $P_{V_{1(2)}}$. This is similar to the experiment described by Ref.¹³, where spin transitions in a DQD with a strong spin-orbit coupling are induced by a classical microwave field applied locally on the DQD, and read out through the charge coupling to a coplanar cavity. However, an important difference with Ref.¹³ is that the present work considers a transport situation. This induces important qualitative modifications of $\Delta\omega_{pull}$, as discussed below. The presence of an anticrossing due to the resonance $\omega_2 = \omega_{V_1 V_2}$ witnesses the existence of a coherent coupling in the system. I show below that the characteristics of $\Delta\omega_{pull}$ and ΔI point to the coherent injection of split Cooper pairs.

B. Case with no relaxation inside the \mathcal{E} subspace

One can first neglect relaxation inside \mathcal{E} , i.e. $M_{rel,cd} = 0$ for any c and d . In this case ΔI is always positive (Fig.2.a) while the sign of $\Delta\omega_{pull}$ varies with δ (Fig.2.b). To understand this result, one must note that the state of \mathcal{E} which is the closest to $|0, 0\rangle$ represents a blocking state for electronic transport, because it has the weakest ability to emit electrons towards the N contacts. One can check that the blocking state is $|V_1\rangle$ for $\delta < 2\Delta_r$ and $|V_2\rangle$ for $\delta > 2\Delta_r$. This is why $|V_1\rangle$ [$|V_2\rangle$] is the most populated state for $\delta < 2\Delta_r$ [$\delta > 2\Delta_r$] (Fig.2.c). Tone 2 always give $\Delta I > 0$ because it induces transitions towards states which can emit electrons more easily. The variation $\Delta\omega_{pull}$ behaves differently because ω_{pull} is proportional to $P_{V_1} - P_{V_2}$ (see Eq. 11). I first discuss $\Delta\omega_{pull}$ along the $|V_1\rangle \rightleftharpoons |V_2\rangle$ resonance. For $\delta < 2\Delta_r$, one has $P_{V_1} > P_{V_2}$ for $\varepsilon_2 = 0$. Since tone 2 tends to equilibrate P_{V_1} and P_{V_2} when ε_2 increases (i.e. $P_{V_1} - P_{V_2} \rightarrow 0$), and since $\mathcal{C} < 0$ for the parameters considered in Fig. 2, one obtains $\Delta\omega_{pull} > 0$. Conversely, for $\delta > 2\Delta_r$, one has $P_{V_1} < P_{V_2}$ for $\varepsilon_2 = 0$, thus $\Delta\omega_{pull} < 0$. Hence, $\Delta\omega_{pull}$ changes sign with δ along the $|V_1\rangle \rightleftharpoons |V_2\rangle$ resonance, at $\delta = 2\Delta_r$. This differs drastically from the usual behavior of a closed two level system coupled dispersively to a cavity, for which $\Delta\omega_{pull}$ has a constant sign, because the state with the lowest energy is always the most populated in the absence of a microwave excitation. Here, electronic transport provides a way to invert the population of the two states $|V_1\rangle$ and $|V_2\rangle$. This is directly visible in $\Delta\omega_{pull}$ which represents a natural probe for the population difference $P_{V_1} - P_{V_2}$. Importantly, the current signal ΔI provides a different information, i.e. it indicates whether tone 2 increases the populations of CPS states with a higher tunnel rate to the N contacts. Note that both $\Delta\omega_{pull}$ and ΔI vanish for $\omega_2 = \omega_{V_1 V_2}$ and $\delta = 2\Delta_r$ because the states $|V_1\rangle$ and $|V_2\rangle$ play symmetric roles at this point.

The resonance $|V_1\rangle \rightleftharpoons |V_2\rangle$ is broad because the coupling constant $\varepsilon_{2,V_1 V_2}$ between tone 2 and this transition is large, hence this transition is saturated, or in other terms, tone 2 leads to $P_{V_1} = P_{V_2}$ for $\omega_2 = \omega_{V_1 V_2}$. In contrast, the resonances $|T_{\pm}\rangle \rightleftharpoons |V_{1(2)}\rangle$ appear as thinner lines because they are not saturated since $\varepsilon_{2,V_1 T_{\pm}}, \varepsilon_{2,T_{\pm} V_1} \ll \varepsilon_{2,V_1 V_2}$ (see Fig.2). Spin-orbit coupling enables tone 2 to populate the states $|T_{\pm}\rangle$ which are unoccupied for $\varepsilon_2 = 0$. This is why one keeps $\Delta\omega_{pull} > 0$ along the $|V_1\rangle \rightleftharpoons |T_{\pm}\rangle$ resonance and $\Delta\omega_{pull} < 0$ along the $|V_2\rangle \rightleftharpoons |T_{\pm}\rangle$ resonance, for any value of δ . Furthermore, ΔI_{CPS} remains positive along both resonances, because the triplet states have no $|0, 0\rangle$ component, and they thus emit electrons to the N reservoirs faster than $|V_{1(2)}\rangle$, for any δ .

When one applies a DC magnetic field B to the circuit, the resonant lines involving the triplet states split into two lines due to Eq. (6), while the $|V_1\rangle \rightleftharpoons |V_2\rangle$ resonances are unchanged because they involve the singlet state (Fig.3). Using $B \neq 0$ can thus be instrumental

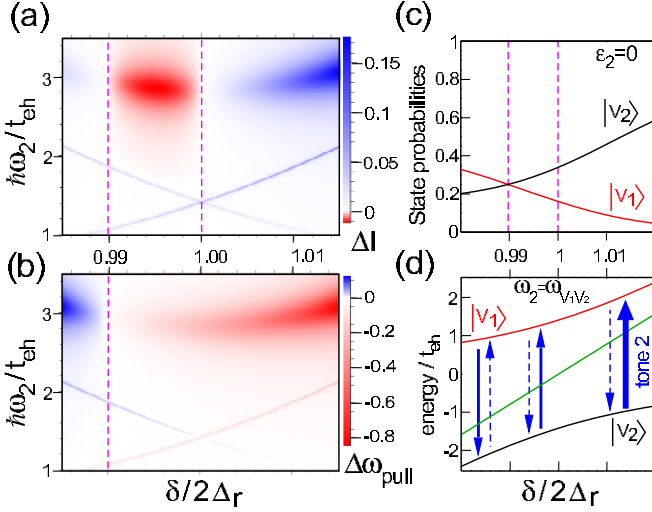


FIG. 4: (a) Current variation ΔI versus δ and ω_2 for a strong relaxation between $|V_1\rangle$ and $|V_2\rangle$ (b) Corresponding $\Delta\omega_{pull}$ (c) Occupation probabilities of states $|V_1\rangle$ and $|V_2\rangle$ for $\varepsilon_2 = 0$ (d) Scheme illustrating that tone 2 decreases the population of the lowest state $|V_2\rangle$, around $\delta = 2\Delta_r$. We have used the same parameters as in Fig.1, $r = 0.55\Gamma_N$ and $\varepsilon_B = 0$.

to reveal the spin structure of the system in an experiment, and confirm that the anticrossing given by the $|V_1\rangle \rightleftharpoons |V_2\rangle$ resonance is due to the injection of spin singlet Cooper pairs.

C. Effect of relaxation between the states $|V_1\rangle$ and $|V_2\rangle$

In practice, relaxation and dephasing can occur between the different CPS states. Dephasing should only modify the visibility of the resonant lines, through Eq.(14). In contrast, relaxation could induce qualitative modifications of ΔI and $\Delta\omega_{pull}$. For simplicity, in the following, I use $M_{rel,V_2V_1} = r$ and the other elements of M_{rel} equal to 0, because $|V_1\rangle$ and $|V_2\rangle$ have the same spin symmetry, thus the transition $|V_1\rangle \rightleftharpoons |V_2\rangle$ should be vulnerable to relaxation induced e.g. by phonons. Figure 4 shows ΔI and $\Delta\omega_{pull}$ for the same parameters as in Fig.2, and r finite. Around $\delta = 2\Delta_r$, $|V_2\rangle$ is the most populated state. Hence, ΔI now changes sign along the $|V_1\rangle \rightleftharpoons |V_2\rangle$ resonance at the point $\delta = 2\Delta_r$, while $\Delta\omega_{pull}$ remains negative. If $r < 2\Gamma_N$, a sign change of $\Delta\omega_{pull}$ persists (see Fig.4.b) for a value of δ smaller than $2\Delta_r$, where $P_{V_1}|\varepsilon_2=0 = P_{V_2}|\varepsilon_2=0$ (see Fig.4.c). This effect goes together with a second sign change of ΔI (Fig.4.a). If $r > 2\Gamma_N$, $\Delta\omega_{pull}$ keeps a constant sign along the whole $|V_1\rangle \rightleftharpoons |V_2\rangle$ resonance (not shown). However, even for $r \gg \Gamma_N$, $\Delta\omega_{pull}$ shows a strong asymmetry with respect to $\delta = 2\Delta_r$, similar to what shown in Fig.4.b for $\delta/2\Delta_r > 0.99$, because $|V_2\rangle$ is the blocking state for $\delta > 2\Delta_r$ only. Hence, even in the presence of internal

relaxation in the CPS, $\Delta\omega_{pull}$ shows a behavior which is very specific to a transport situation.

D. Expected amplitude of the signals

It is important to point out that the above effects are already within experimental reach. Joint measurements of the current through a nanocircuit and the corresponding cavity frequency pull are now realized commonly in experiments combining nanocircuits and coplanar microwave cavities^{11,12,14}. For the realistic parameters used in Figs. 2, 3 and 4 (see Refs.^{2,24-26}), the magnitude of $\Delta\omega_{pull}[\Delta I]$ is set by the scales $\omega_0 \sim 2\pi \times 40\text{kHz}$ [$e\Gamma_N \sim 20\text{pA}$]. Hence, these signals are accessible experimentally with present techniques¹⁴. The above model and parameters are compatible with cavity quality factors $Q \sim 1000$ obtained presently in Hybrid Circuit QED. This work considers CNT-based devices which are the most advanced systems for Cooper pair splitting³, but similar results are expected with other types of nanoconductors.

IV. CONCLUSION

To summarize, Hybrid Circuit QED provides a direct access to the coherence of Cooper pair injection in the CPS. This coherence is revealed by an anticrossing in the cavity frequency pull, which can be discriminated from all other possible anticrossings because of various unusual specificities. First, this anticrossing is visible along the δ axis, which necessarily points to processes involving electron pairs split between the two dots. Second, it displays sign changes or asymmetries with δ , which reveal a population inversion due to out-of-equilibrium transport. This property is difficult to mimic without an exchange of particles with a superconducting reservoir. Third, the splitting of the cavity frequency pull with a magnetic field reveals the spin structure of the two-particle states involved. Note that these results do not represent a direct proof for the conservation of spin entanglement in the CPS, but it seems unlikely to have spin entanglement conservation without coherent pair injection. Observing the coherent pair injection through the cavity frequency pull can thus be an instrumental step towards the realization of a fully coherent CPS. More generally, this work illustrates that Hybrid Circuit QED provides a rich tool to study electronic transport in nanostructures.

Note that the present work considers a limit where one can disregard single quasiparticle transport from the superconducting contact to the dots, as well as Cooper pair injection in a single dot or other parasitic processes⁶. In a real experiment, these processes could become significant depending on the device parameters. Nevertheless, this should modify only quantitatively the properties of the anticrossing induced by t_{eh} , if one achieves a sufficient Cooper pair splitting rate.

I acknowledge fruitful discussions with T. Kontos. This work has been financed by the EU-FP7 project SE2ND[271554] and the ANR Nanoquartet.

V. APPENDIX A: EXPRESSION OF THE CPS EIGENSTATES

I note $|\tau\sigma, \tau'\sigma'\rangle$ the CPS state with one electron with spin σ in orbital τ of dot L and one electron with spin σ' in orbital τ' of dot R . By definition, the spin states $\sigma \in \{\uparrow, \downarrow\}$ are along the carbon nanotube axis, and parallel to the effective field \tilde{h}_{so} produced by the spin orbit coupling (term in Δ_{so}). The five eigenstates of the subspace \mathcal{E} discussed in the main text are:

$$|V_1\rangle = \sqrt{1 - v_1^2} |0, 0\rangle + v_1 |\mathcal{S}\rangle \quad (15)$$

$$|V_2\rangle = \sqrt{1 - v_2^2} |0, 0\rangle + v_2 |\mathcal{S}\rangle \quad (16)$$

$$|T_{-1}\rangle = (|\mathcal{T}_0\rangle - |\mathcal{T}_{-}\rangle)/\sqrt{2} \quad (17)$$

$$|T_{+1}\rangle = (|\mathcal{T}_0\rangle + |\mathcal{T}_{-}\rangle)/\sqrt{2} \quad (18)$$

$$|T_0\rangle = |\mathcal{T}_{+}\rangle \quad (19)$$

Above, the state $|\mathcal{T}_0\rangle$ correspond to a generalized triplet state with zero spin along the nanotube axis, and $|\mathcal{T}_{+}\rangle$ and $|\mathcal{T}_{-}\rangle$ correspond to coherent superpositions of triplet states with equal spins, i.e.

$$|\mathcal{S}\rangle = \sum_{\sigma} \left\{ \frac{1}{2} \left(\frac{\Delta_{so}}{\Delta_r} - \sigma \right) |\mathcal{C}_{-}(K\sigma, K'\bar{\sigma})\rangle \right\} \quad (20)$$

$$+ \frac{\Delta_{K/K'}}{2\Delta_r} \sum_{\tau} |\mathcal{C}_{-}(\tau \uparrow, \tau \downarrow)\rangle \quad (21)$$

$$|\mathcal{T}_0\rangle = \sum_{\sigma} \frac{1}{2} \left(\sigma \frac{\Delta_{so}}{\Delta_r} - 1 \right) |\mathcal{C}_{+}(K\sigma, K'\bar{\sigma})\rangle \quad (22)$$

$$+ \frac{\Delta_{K/K'}}{2\Delta_r} \sum_{\tau} |\mathcal{C}_{+}(\tau \uparrow, \tau \downarrow)\rangle \quad (23)$$

$$|\mathcal{T}_{+}\rangle = \sum_{\sigma} \frac{1}{2} \left(\frac{\Delta_{so}}{\Delta_r} - \sigma \right) \frac{|K\sigma, K\sigma\rangle - |K'\bar{\sigma}, K'\bar{\sigma}\rangle}{\sqrt{2}} \quad (24)$$

$$+ \sum_{\sigma} \sigma \frac{\Delta_{K/K'}}{2\Delta_r} |\mathcal{C}_{+}(K\sigma, K'\sigma)\rangle \quad (25)$$

$$|\mathcal{T}_{-}\rangle = \sum_{\sigma} \frac{1}{2} \left(1 - \frac{\Delta_{so}}{\Delta_r} \sigma \right) \frac{|K\sigma, K\sigma\rangle + |K'\bar{\sigma}, K'\bar{\sigma}\rangle}{\sqrt{2}} \quad (26)$$

$$- \sum_{\sigma} \frac{\Delta_{K/K'}}{2\Delta_r} |\mathcal{C}_{+}(K\sigma, K'\sigma)\rangle \quad (27)$$

and

$$v_{1(2)} = \frac{2t_{eh}}{\sqrt{8t_{eh}^2 + d(d \mp \sqrt{8t_{eh}^2 + d^2})}} \quad (28)$$

with $d = \delta - 2\Delta_r$. I have used above $|\mathcal{C}_{\pm}(\tau\sigma, \tau'\sigma')\rangle = (|\tau\sigma, \tau'\sigma'\rangle \pm |\tau'\sigma', \tau\sigma\rangle)/\sqrt{2}$. Note that $\sigma = \pm 1$ stands for spin states $\sigma \in \{\uparrow, \downarrow\}$ in algebraic expressions, with $\bar{\sigma} = -\sigma$. The eigenstates $|T_{-1}\rangle$ and $|T_{+1}\rangle$ of the full system correspond to a superposition of $|\mathcal{T}_0\rangle$ and $|\mathcal{T}_{-}\rangle$, due to the presence of the magnetic field \vec{B} which is perpendicular to \tilde{h}_{so} .

VI. APPENDIX B: APPROXIMATIONS

This section discusses various approximations used in the main text.

A. Photon-induced transition between CPS singly occupied states

Photon-induced transition inside the CPS singly occupied charge sector could modify $\Delta\omega_{cav}$ and the reaction of the CPS to tone 2, in principle. To discuss this possibility it is useful to recall that one has typically $t_{ee}, \Delta_r \gg t_{eh}, \hbar\omega_{cav}$. I furthermore assume that $\varepsilon_B \ll \hbar\omega_{cav}, \hbar\omega_2$. One can check that photon-induced transitions inside the CPS singly occupied charge sector correspond to frequencies of the order of $2\Delta_r, 2t_{ee}$, or ε_B . The two first values are typically too large and the last one too small to enable an excitation inside the singly occupied charge sector by tone 2, because of the limited frequency range of microwave sources ($\hbar\omega_2 \ll t_{ee}, \Delta_r$) and because I assume $\hbar\omega_2 \gg \varepsilon_B$. Regarding $\Delta\omega_{pull}$, one can expect a significant contribution from the charge couplings $\lambda_{L(R)}$ only. One can check that photon-induced transitions corresponding to $\lambda_{L(R)}$ have frequencies $2t_{ee}$ which is typically huge compared to t_{eh} and $\hbar\omega_{cav}$. Therefore the contribution of these transitions to $\Delta\omega_{pull}$ can be disregarded in comparison with the contribution (11) from the main text.

B. RWA on independent resonances

The RWA on independent resonances requires that the various resonances induced by tone 2 are sufficiently separated. This is not justified at the crossing between the different thin resonances in Figs.2 to 4. Nevertheless, corrections are expected in a very small fraction of the parameters space, barely visible in Figs. 2 to 4. The related physics goes beyond the scope of this article.

C. CPS/cavity coupling elements

For simplicity, Eq.(4) of the main text restricts the symmetry of the spin-flip and orbit-change terms of h_c . There can be extra terms with other symmetries, depending on the microscopic details of the carbon nanotube quantum dots. The terms used in the main text lead to

the most interesting effects expected in the CPS/cavity system. For the spin-flip terms in h_c , extra contributions in $\mathbf{i}\sigma\tau\tilde{\lambda}_i d_{i\tau\sigma}^\dagger d_{i\tau\bar{\sigma}}$ or $\tau\tilde{\lambda}_i d_{i\tau\sigma}^\dagger d_{i\tau\bar{\sigma}}$ are compatible with the hermicity of H_{tot} , but this does not modify the coupling between the states of \mathcal{E} . An extra contribution in $\tilde{\lambda}_i d_{i\tau\sigma}^\dagger d_{i\tau\bar{\sigma}}$ would add couplings $\alpha_{T_0 V_1(2)} = v_{1(2)} \mathbf{i}(\tilde{\lambda}_L - \tilde{\lambda}_R) \Delta_{K \leftrightarrow K'} / \Delta_r$ between the states $|V_{1(2)}\rangle$ and $|T_0\rangle$. This could produce extra thin resonant lines in Figs. 3.a and 3.b for $\omega_2 = \omega_{V_1 T_0}$ and $\omega_2 = \omega_{T_0 V_2}$. This effect can be included straightforwardly in the system description.

For the photon-induced orbit-changes, an imagi-

nary contribution to h_c with the form $\mathbf{i}\tau\tilde{\alpha}_i d_{i\tau\sigma}^\dagger d_{i\tau\bar{\sigma}}$ or $\mathbf{i}\tau\tilde{\alpha}_i d_{i\tau\sigma}^\dagger d_{i\tau\bar{\sigma}}$ is possible, in principle, but this does not modify the coupling between the states of \mathcal{E} . A contribution with the form $\tilde{\alpha}_i \sigma d_{i\tau\sigma}^\dagger d_{i\tau\bar{\sigma}}$ would lead to a renormalisation of Eqs.(8) and (9), i.e. one should replace $\mp \mathbf{i}(\lambda_L - \lambda_R)$ by $\mp \mathbf{i}(\lambda_L - \lambda_R) + (\tilde{\alpha}_L - \tilde{\alpha}_R)$ and $\mathbf{i}(\lambda_L + \lambda_R)$ by $\mathbf{i}(\lambda_L + \lambda_R) + (\tilde{\alpha}_L + \tilde{\alpha}_R)$. This would affect only quantitatively the results presented in this paper. In any case, the CPS/cavity charge couplings $\beta_{L(R)}$ are expected to be dominant, so that the spin-flip and orbit-change couplings will not affect the $|V_1\rangle \rightleftharpoons |V_2\rangle$ resonance, but rather control the thin resonant lines in Figs. 2 to 4.

-
- ¹ P. Recher, E. V. Sukhorukov, and D. Loss, Phys. Rev. B **63**, 165314 (2001).
 - ² L. Hofstetter et al., Nature **461**, 960 (2009); L. G. Herrmann et al., Phys. Rev. Lett. **104**, 026801 (2010); L. Hofstetter et al., Phys. Rev. Lett. **107**, 136801 (2011); J. Schindele et al., Phys. Rev. Lett. **109**, 157002 (2012), L. G. Herrmann et al., arXiv:1205.1972; A. Das, et al., Nature Communications 3, Article number: 1165 (2012).
 - ³ J. Schindele et al., Phys. Rev. B, **89**, 045422 (2014)
 - ⁴ T. Martin, Phys. Lett. A **220**, 137 (1996); M. P. Anantram and S. Datta, Phys. Rev. B **53**, 16390 (1996); G. Burkard, D. Loss, and E. V. Sukhorukov, Phys. Rev. B **61**, R16303 (2000); S. Kawabata, J. Phys. Soc. Jpn. **70**, 1210 (2001); G. B. Lesovik, T. Martin, and G. Blatter, Eur. Phys. J. B **24**, 287 (2001)
 - ⁵ A. Schroer et al., arXiv:1404.4524
 - ⁶ O. Sauret et al., Phys. Rev. B **70**, 245313 (2004).
 - ⁷ J. Eldridge, et al., Phys. Rev. B **82**, 184507 (2010).
 - ⁸ H. Mabuchi and A. Doherty, Science **298**, 1372 (2002).
 - ⁹ J.M. Raimond, M. Brune and S. Haroche, Rev. Mod. Phys. **73**, 565 (2001).
 - ¹⁰ A. Wallraff et al. Nature **431**, 162 (2004).
 - ¹¹ M.R. Delbecq, et al. Phys. Rev. Lett. **107**, 256804 (2011); M.R. Delbecq et al., Nature Communications **4**, Article number: 1400 (2013).
 - ¹² T. Frey, et al., Phys. Rev. Lett. **108**, 046807 (2012); M. D. Schroer et al., Phys. Rev. Lett. **109**, 166804 (2012); H. Toida, T. Nakajima, and S. Komiyama, Phys. Rev. Lett. **110**, 066802 (2013); J. Basset et al., Phys. Rev. B **88**, 125312 (2013); G.-W. Deng et al., arXiv:1310.6118.
 - ¹³ K. D. Petersson, et al., Nature **490**, 380 (2012).
 - ¹⁴ J.J. Viennot et al., Phys. Rev. B **89**, 165404 (2014).
 - ¹⁵ A. Cottet et al., Semicond. Sci. Technol. **21**, S78 (2006).
 - ¹⁶ S. De Franceschi et al., Nature Nanotechnology **5**, 703 (2010).
 - ¹⁷ M. Trif, et al., Phys. Rev. B **77**, 045434 (2008); A. Cottet and T. Kontos, Phys. Rev. Lett. **105**, 160502 (2010); P.-Q. Jin et al., Phys. Rev. Lett. **108**, 190506 (2012); X. Hu et al., Phys. Rev. B **86**, 035314 (2012); C. Kloeffer et al., Phys. Rev. B **88**, 241405(R) (2013).
 - ¹⁸ A. Cottet, T. Kontos, and A. Levy Yeyati, Phys. Rev. Lett. **108**, 166803 (2012).
 - ¹⁹ M. Trif and Y. Tserkovnyak, Phys. Rev. Lett. **109**, 257002 (2012); A. Cottet, T. Kontos and B. Douçot, Phys. Rev. B **88**, 195415 (2013); T. L. Schmidt, A. Nunnenkamp, and C. Bruder, Phys. Rev. Lett. **110**, 107006 (2013).
 - ²⁰ F. Hassler et al., New J. Phys. **13**, 095004 (2011); T. Hyart et al., Phys. Rev. B **88**, 035121 (2013); C. Müller, J. Bourassa and A. Blais, Phys. Rev. B **88**, 235401 (2013); E. Ginossar and E. Grosfeld, arXiv 1307.1159.
 - ²¹ Childress, et al., Phys. Rev. A **69**, 042302 (2004); Jin et al, Phys. Rev. B **84**, 035322 (2011); M. Kulkarni, O. Cotlet, and H. E. Türeci, arXiv:1403.3075.
 - ²² C. Bergenfeldt et al., Phys. Rev. B **87**, 195427 (2013); N. Lambert et al., Europhys. Lett. **103**, 17005 (2013); L. D. Contreras-Pulido et al., New Journal of Physics **15**, 095008 (2013), C. Bergenfeldt et al., Phys. Rev. Lett. **112**, 076803, (2014).
 - ²³ Y.-Y. Liu et al., Phys. Rev. Lett. **113**, 036801 (2014)
 - ²⁴ T. S. Jespersen et al., Nature Physics **7**, 348 (2011).
 - ²⁵ W. Liang, M. Bockrath, and H. Park, Phys. Rev. Lett. **88**, 126801 (2002).
 - ²⁶ F. Kuemmeth, et al. Nature **452**, 448 (2008).
 - ²⁷ A. Pályi and G. Burkard, Phys. Rev. B **82**, 155424 (2010); A. Pályi and G. Burkard, Phys. Rev. Lett. **106**, 086801 (2011).
 - ²⁸ A. Cottet et al., to be published elsewhere.
 - ²⁹ A. Cottet, Phys. Rev. B **86**, 075107 (2012).